TM-1145
1183.000
Nov. 1982

Scaling Neutron Absorbed Dose Distributions From One Medium to Another

M. Awschalom, I. Rosenberg, R. K. Ten Haken

Fermilab Neutron Therapy Facility, P. O. Box 500, Batavia, IL 60510

ABSTRACT

Central axis depth dose (CADD) and off-axis absorbed dose ratio (OAR) measurements were made in water, muscle and whole skeletal bone TE-solutions, mineral oil and and glycerin with a clinical neutron therapy beam. These measurements show that, for a given neutron beam quality and field size, there is a universal CADD distribution at infinity if the depth in the phantom is expressed in terms of appropriate scaling lengths. These are essentially the kerma-weighted neutron mean free paths in the media. The method used in ICRU #26 to scale the CADD by the ratio of the densities is shown to give incorrect results. The OAR's measured in different media at depths proportional to the respective mean free paths were also found to be independent of the media to a good approximation.

Therefore, neutron beam CADD's and OAR's may be measured in either TE-solution (USA practice) or water (European practice), and having determined the respective scaling lengths, all measurements may be scaled from one medium to any other. It is recommended that for general treatment planning purposes, scaling be made to TE-muscle with a density of 1.04 g cm^{-3}, since this value represents muscle and other soft tissues better than TE-solution of density 1.07 g cm^{-3}. For such a transformation, relative measurements made in water are found to require very

small corrections. Hence, it is further recommended that relative CADD and OAR measurements be performed in water because of its universality and convenience. Finally, a table of calculated scaling lengths is given for various neutron energy spectra and for various tissues and materials of practical importance in neutron dosimetry.

KEY WORDS: Dosimetry, neutrons, CADD, OAR, phantom, treatment planning, scaling.

INTRODUCTION

Adopted procedures for neutron beam dosimetry differ in several major respects between the USA and Europe. The AAPM Task Group on Neutron Dosimetry[1] recommends that neutron dose distributions be measured in a tissue-equivalent (TE) liquid and be reported as total (n+γ) doses. The European Protocol on Neutron Beam Dosimetry,[2] on the other hand, recommends measurements in water and separation of the dose into neutron and photon components.

Neither water nor the recommended TE-solutions,[3,4] in fact, have the correct density and/or composition with respect to soft tissues. Most tissues listed in ICRP 23,[5] including muscle, liver and kidney, have densities varying between 1.03 and 1.05 g cm^{-3}, as opposed to the densities of many TE materials, 1.07 g cm^{-3} to 1.12 g cm^{-3}. Thus, some correction should be made to the measured dose distributions in phantom media to obtain the correct distributions in tissues. The suggestion in ICRU 26[6] that measurements from one medium be transferred to another through scaling by densities is shown not to be satisfactory even in the example used in that reference.

To examine the significance of different phantom materials, and the relationship between them, central axis depth dose (CADD), off-axis absorbed dose ratio (OAR), and kerma attenuation measurements were made in several liquid media with a clinical neutron therapy beam.

ASSUMPTIONS AND METHOD

The relative central axis depth dose in phantom of a neutron or photon beam can always be expressed as the product of a medium-related attenuation function and a purely geometrical factor:

$$CADD(ESQ,SSD,z) = \frac{F\left(ESQ,\frac{z}{\ell}\right)}{F\left(ESQ,\frac{z_m}{\ell}\right)} \frac{(SSD+z_m)^2}{(SSD+z)^2} \qquad (1)$$

where ESQ is the beam cross-section equivalent square at the surface of the phantom, SSD in the source-to-surface distance, z is the depth in the phantom and z_m is the depth for maximum dose. The function F will be recognized as the central axis depth dose for the source at infinity ($CADD_\infty$), normalized to unity at z_m by the factor $F(ESQ,\frac{z_m}{\ell})$. It is shown as a function of ESQ and z/ℓ, where ℓ is some characteristic length for the medium and the neutron energy spectrum. With an appropriate choice of ℓ, the

scaling length, the function F should become independent of medium for depths larger than z_m, when expressed in terms of z/ℓ. If these scaling lengths were known for various media, then it would be possible to transfer dose distribution measurements obtained in a medium to another one.

The first characteristic length that suggests itself for ℓ is the kerma-weighted neutron mean free path in the medium. This can be calculated from a knowledge of the elemental composition of the medium, the neutron energy spectrum, the elemental kerma functions and the elemental total neutron cross-sections (Appendix A).

Another possible characteristic length is the initial narrow beam kerma attenuation length for the medium and the neutron energy spectrum.[7] Therefore, narrow beam transmission measurements were also performed in each medium for the neutron beam used in this study. Other suggested characteristic lengths are related to the mass per unit area (ICRU 26[6]) and mass of hydrogen per unit area.

Finally, the above assumptions and the suitability of proposed characteristic lengths were tested by obtaining the most appropriate scaling factors from $CADD_\infty$ distributions measured in the various media.

EXPERIMENTAL PROCEDURES

The measurements were made using the p(66)Be(49) fast neutron therapy beam at the Fermilab Neutron Therapy Facility.[8,9] The facility, phantom, remotely controlled positioner, electronics for charge collection and digitizing, and automated continuous data correction used for the CADD and OAR measurements have been described previously.[9-12] In brief, positional precision in depth of $\pm$0.5 mm and relative dose measurement precision of $\pm$0.5% were easily achieved.

Five liquid phantom media were investigated: water, muscle[4] and whole skeleton[13] TE-solutions, motor oil[14] and glycerin. These liquids were chosen for their wide range of densities and elemental compositions (Table 1).

CADD's and OAR's were measured in a lucite phantom filled in turn with each liquid under investigation. Six field sizes (from 8x8 to 24x24 cm^2) at SSD's varying from 143 to 220 cm, and various ionization chambers were used. These air-filled, A-150 plastic[15] ionization chambers were: a parallel plate chamber[16] or a 0.5 cm^3 thimble chamber[17] for the CADD measurements, and a 0.1 cm^3 thimble chamber[18] for the OAR scans. However, for a given field size, the same chamber was used in all liquid media.

For narrow beam[19] kerma attenuation measurements a partitioned trough was made of thin stainless steel sheets. It could accommodate beams having cross-sections of up to 10x15 cm^2. The thicknesses of fluid absorber could be increased in steps of 2.54 cm. The kerma attenuation of the beam by the partitions in the trough was about 5%, and had only a small hardening effect on the neutron beam.[20] The detector used for these measurements was an air filled 1.0 cm^3 A-150 ionization chamber[21] with build-up cap of the same material located 330 cm from the target and 220 cm from the upstream end of the trough. The transmission through varying thicknesses of all five liquids under investigation was measured for different field sizes, ranging from 5x5 to 10x10 cm^2 at the detector (1.7 x 1.7 to 3.5 x 3.5 cm^2 at the trough). No dependence on field size of the transmitted kerma fractions was found, indicating that acceptable narrow beam geometry had been achieved.

RESULTS AND ANALYSIS

Measurements of central axis depth dose converted to infinite SSD ($CADD_\infty$'s) for a representative 14 x 14 cm^2 field size are shown for all five liquid phantoms in Fig. 1, where depth is given in centimeters. Each set of measurements was normalized to unity at its maximum dose. It may be seen that the depths for maximum dose are practically the same for all liquids, while the $CADD_\infty$'s diverge past the maximum.

The $CADD_{\infty}$ curves expressed in terms of mass per unit area (Fig. 2) and of mass of hydrogen per unit area (Fig. 3) also diverge from each other past the maximum. Clearly, these transformations do not lead to a medium-independent $CADD_{\infty}$ function. As mentioned before, expressing $CADD_{\infty}$'s as functions of depth measured in units of either kerma attenuation lengths or neutron mean free paths may provide alternative methods of obtaining medium-independent $CADD_{\infty}$'s. To determine these characteristic lengths, kerma transmission measurements and mean free path calculations were performed for the p(66)Be(49) neutron beam.

The kerma fractions transmitted through varying thicknesses of liquids are shown in Fig. 4. Substantial hardening of the beam occurs in the first thicknesses of absorber and the kerma transmission curves soon deviate from a simple exponential. Initial kerma attenuation lengths (Λ) were obtained from the initial slopes of the attenuation curves,[7] using the first measured thickness only (Table 2). The ratios of attenuation length in water to that in the other media, $\Lambda(\text{water})/\Lambda(\text{liquid})$, are given in Table 3. Different attenuation lengths were also obtained from the measurements shown in Fig. 4, using the asymptotic slopes of the curves at larger absorber thicknesses. These values were larger than the ones shown in Table 2, but the $\Lambda(\text{water})/\Lambda(\text{liquid})$ values obtained from them were the same, within two percent, as those listed (Table 3) for all liquids. Thus,

these ratios are seen to be characteristic of the media. Calculated detector-dependent attenuation lengths (Appendix A) are also shown in Table 2. The calculated and measured initial attenuation lengths agree with each other to within three percent, which is remarkable in the light of the uncertainties involved. This agreement gives confidence to the mean free path calculations (Table 4).

The kerma-weighted neutron mean free paths (λ) for all liquids were calculated for the p(66)Be(49) neutron beam (Appendix A). The neutron energy spectrum for this beam and the elemental kerma functions were taken from a recent review of neutron kerma values.[22] Total elemental cross-sections were taken from reference 23. The results of these calculations are shown in Table 4, while the ratios λ(water)/λ(liquid) are given in Table 3.

Now the $CADD_{\infty}$ data may also be expressed in units of measured initial attenuation lengths (Fig. 5) or calculated mean free paths (Fig. 6) for each medium. These transformations make the $CADD_{\infty}$'s nearly independent of medium.

It is also desirable to obtain the best possible scaling factors from the $CADD_{\infty}$ measurements themselves and compare them with those obtained using the above characteristic lengths. This can be done by empirically choosing scaling lengths, ℓ, for each medium such that the $CADD_{\infty}$ expressed in units of these lengths are

congruent within the uncertainties of the measurements (Appendix B).

The resulting values of the optimum scaling factor from water to a medium j, SF_{wj}[= ℓ(water)/ℓ(liquid)] are shown in Table 3, and the $CADD_{\infty}$ data for the 14 x 14 cm^2 field expressed in units of the resulting scaling lengths ℓ are shown in Fig. 7. The values of ℓ were the same, within one percent, for all measured field sizes in each medium, and thus they are characteristic of each medium.

Measurements of off-axis ratios were also made in most liquids under study with a 9X9 cm^2 field size at an SSD of 143 cm. The depths were determined to correspond to 10 cm of water using the ratios of λ's (Table 3) as scaling factors. After allowing for geometrical divergences, the OAR's in the different media were practically indistinguishable from each other (Fig. 8). This means that, if an $OAR(x,z,z_{eff},W)$ algorithm is determined in liquid j as a function of off-axis distance x, tissue depth z_{eff} (equal to geometrical depth z) and nominal width W at that depth,[11] then the same algorithm will apply in liquid k if tissue depth is scaled as $z_{eff} = z(\lambda_k/\lambda_j)$ in the second liquid, while the actual depth z is used to determine the geometrical width W and the width of the penumbra by dual projection scaling.[11]

DISCUSSION AND CONCLUSIONS

Since the values of the optimum scaling factors have been obtained empirically by measuring the CADD's in several media, it would be useful to be able to predict the scaling factors for other media, especially tissues, where direct measurements are difficult. Of the various suggested criteria (Table 3), the ratios of calculated λ's comes closest to predicting the optimal scaling factors for a wide range of densities and elemental compositions. Density ratios and hydrogen density ratios, sometimes proposed as scaling criteria, are seen to predict incorrect scaling factors. The ratios of measured kerma attenuation lengths Λ come closer, at least for some of the media studied here, but the difficulties in determining the attenuation properties of tissues and organs are even greater than for liquid media.

The effect of 1-2% changes in the scaling factors and the errors involved in the use of λ's instead of ℓ's in determining these factors are illustrated in the curves of $CADD_\infty$ ratios to water shown in the upper part of Fig. 9 (Appendix B). Errors of less than 2.5% will occur, and only at depths corresponding to about 20 cm of water, even when the ratio of λ's differs by 2% from the optimum scaling factor (Table 3). In fact, in the scale of Fig. 6 the agreement among the various curves is satisfactory, though not as good as in Fig. 7.

In view of the above results, the kerma-weighted neutron mean free path calculations (Appendix A) are proposed for predicting scaling lengths of different media. Following this recommendation, the mean free paths in several tissues and materials useful for dosimetry have been calculated for several neutron therapy beams currently or soon to be in clinical use (Table 4). Large uncertainties may exist in the knowledge of tissue compositions, elemental kerma functions and neutron energy spectra used in these calculations.[22] These uncertainties were discussed in the paper from which these quantities were taken.[22] It was shown there that, when ratios of average kermas were considered, the resulting total uncertainties were relatively small. Thus, it is expected that the uncertainties in the values of scaling factors, which are obtained as ratios of two lengths calculated using the same basic data, should also be relatively small. Confidence in the above calculations is also reinforced by their success in predicting initial kerma attenuation lengths (Table 2). Furthermore, as shown above, deviations of as much as $\pm$2% from the optimal scaling values introduce only very small errors in predicted relative doses. The above calculations predict that the scaling factors from TE solutions to water $\lambda(TE)/\lambda(water)$, among others, vary somewhat among the various neutron beams, and it would be interesting to measure these scaling factors experimentally.

Materials of almost identical elemental composition but of different density, such as ICRU muscle[6] and muscle TE-solution,[4] have a scaling factor to each other equal to the inverse ratio of their densities. Therefore, if CADD measurements are performed in a TE-solution of density 1.07 g cm^{-3}, a scaling factor of $(1.07/1.04)^{-1} = 0.97$ is necessary in Eq. B4 to predict absorbed doses to patients muscle tissue or most soft organs,[5,13] whose densities vary between 1.03 and 1.05 g cm^{-3}. Alternatively, a tissue substitute liquid of the correct density could be used for measurements,[13] with no need of scaling to human muscle. For most neutron spectra calculated here, however, the ratio of mean free paths of ICRU muscle to water is very close to unity (Table 4). Thus, it appears that, at least for relative dosimetry, the direct use of water-acquired data in treatment planning calculations is fortuitously close to being correct.

RECOMMENDATION

Recognizing that muscle and internal organ tissues have densities of 1.03 to 1.05 g cm^{-3}, CADD's and OAR's measured in TE-solution of ρ = 1.07 g cm^{-3} should be scaled to ρ = 1.04 g cm^{-3} for patient calculations. However, measurements of relative dose distributions in water, which has advantages over TE-solutions, may be used directly for patient calculations and treatment planning with acceptable errors.

ACKNOWLEDGEMENT

This investigation was supported by PHS Grant Number 5P01CA18081-08 awarded by the National Cancer Institute, DHHS. We thank Ms. Michelle Gleason for accurate typing and infinite patience with the authors.

Table 1

Physical Characteristics of Liquid Phantoms

LIQUID	DENSITY ($g\ cm^{-3}$)	ELEMENTAL COMPOSITION (% BY MASS)†				
		H	C	N	O	Other
Motor Oil[14]	0.88	13.1	85.7	-	-	0.6F
Water	1.00	11.2	-	-	88.8	-
T.E. Solution[4]	1.07	10.2	12.0	3.5	74.3	-
Glycerin	1.25	8.8	39.1	-	52.1	-
Skel. Eq. Sol.[13]	1.40	7.2	13.9	2.9	58.3	7.0P, 10.2K

Note: † Composition from chemical analysis, except for Skeleton Equivalent Solution.

Table 2

Measured and Calculated Initial Kerma Attenuation Lengths Λ

of Liquid Phantoms for p(66)Be(49) Neutrons

LIQUID	MEASURED[a] (cm)	CALCULATED[b] (cm)
Motor Oil	11.8	11.5
Water	11.5	11.2
T.E. Solution	11.0	10.8
Glycerin	9.5	9.6
Skel. Eq. Sol.	9.5	9.6

Notes:

(a) From measurements shown in Fig. 4

(b) Weighted by the kerma response of the detector made of A-150 TE plastic (Appendix A).

Table 3

Comparison of Possible Scaling Factors from

Water to Liquid Phantoms for p(66)Be(49) Neutrons

LIQUID	RATIO OF DENSITIES ρ/ρ(water)	RATIO OF HYDROGEN DENSITIES[a] $\rho H/\rho H$(water)	$\frac{\Lambda(\text{water})}{\Lambda(\text{liquid})}$ [b]	$\frac{\lambda(\text{water})}{\lambda(\text{liquid})}$ [c]	OPTIMAL[d] SCALING FACTOR
Motor Oil	0.88	1.03	0.98	0.98	0.99
T.E. Solution	1.07	0.97	1.05	1.03	1.04
Gylcerin	1.25	0.98	1.22	1.14	1.15
Skel. Eq. Sol.	1.40	0.90	1.21	1.14	1.16

Notes:

(a) Hydrogen density in water = 0.112 g cm^{-3}

$\rho_H = \rho \times m_H$ = density x hydrogen fraction (from Table 1).

(b) Ratios of measured initial attenuation lengths from Table 2.

(c) Ratios of calculated mean free paths from Table 4.

(d) Ratios of empirical scaling lengths ℓ(water)/ℓ(liquid) which make functions $F(\beta = z/\ell)$ in Appendix B independent of medium.

Table 4

Calculated Kerma-Weighted Mean Free Paths (cm) for

Several Media and Neutron Therapy Beams

MATERIALS & TISSUES[a]	DENSITY ($g\ cm^{-3}$)	NEUTRON BEAMS[a]					
		p(66)Be	p(41)Be	d(22)Be	d(16)Be	d+T	d(8.3)D
Motor Oil	0.88	10.79	8.23	7.66	5.39	6.97	7.69
Water	1.00	10.57	8.24	7.71	5.31	6.91	7.91
T.E. Solution	1.07	10.24	7.99	7.51	5.24	6.74	7.70
Glycerin	1.25	9.23	7.22	6.83	4.88	6.15	7.02
Skel.Eq.Sol.	1.40	9.26	7.39	6.99	5.03	6.33	7.19
Muscle[b]	1.04	10.54	8.24	7.74	5.41	6.95	7.93
Bone[c]	1.85	8.08	6.79	6.54	4.92	6.01	6.77
Fat[d]	0.92	10.98	8.45	7.90	5.57	7.16	7.99
Brain	1.03	10.36	8.08	7.57	5.26	6.80	7.75
Lungs	0.26	42.72	33.4	31.5	22.0	28.2	32.3
A-150[e]	1.12	9.56	7.38	6.93	4.98	6.31	7.01
Polyethylene	0.96	9.44	7.18	6.65	4.65	6.06	6.67
Polystyrene	1.06	11.13	8.65	8.23	6.09	7.49	8.40
Lucite	1.20	9.84	7.68	7.30	5.30	6.60	7.49
Nylon[f]	1.14	9.54	7.39	6.93	5.01	6.31	7.04

Notes:

(a) Elemental compositions and neutron energy spectra taken from

standard beams in Ref. 22, except (d+T), for which the degraded spectrum at 2 cm deep was used. Elemental compositions of materials were also taken from Ref. 22. Where alternative choices were given in that reference, the following compositions were chosen:

(b) ICRU muscle.[6]

(c) Cortical bone, (ICRP 23).[5]

(d) Subcutaneous adipose tissue (ICRP 23).[5]

(e) Smathers et al.[15]

(f) Type 6/6.[6]

Figure Captions

Fig. 1. Central axis relative doses corrected to infinite SSD for a 14 x 14 cm^2 field size in different liquid media. Each set of measurements was normalized to unity at its maximum dose. Depth is expressed in centimeters.

Fig. 2. Data from Fig. 1, with depth expressed in g cm^{-2}.

Fig. 3. Data from Fig. 1, with depth expressed in g cm^{-2} of hydrogen.

Fig. 4. Narrow beam kerma attenuation results for different liquid media. Data normalized to unity at zero absorber thickness.

Fig. 5 Data from Fig. 1, with depth, expressed in units of measured kerma attenuation lengths (Table 2).

Fig. 6 Data from Fig. 1, with depth, expressed in units of calculated mean free paths (Table 4).

Fig. 7 Data from Fig. 1, with depth expressed in units of optimal scaling lengths (Appendix B).

Fig. 8 Off-axis ratios in different liquid media, normalized to unity at the central axis. 9 x 9 cm^2 field size at SSD = 143 cm. The depths for each liquid were: water = 10.0 cm; oil = 10.2 cm; TE solution = 9.7 cm; glycerin = 8.8 cm. The results were scaled to 10 cm depth for geometrical divergence before plotting.

Fig. 9. Ratios of data in Fig. 1, relative to the water values, after the transformations described in Appendix B. Upper portion: ratios of depth dose data expressed in units of calculated mean free paths. Lower portion: same ratios obtained after the depth dose data were expressed in units of optimal scaling lengths.

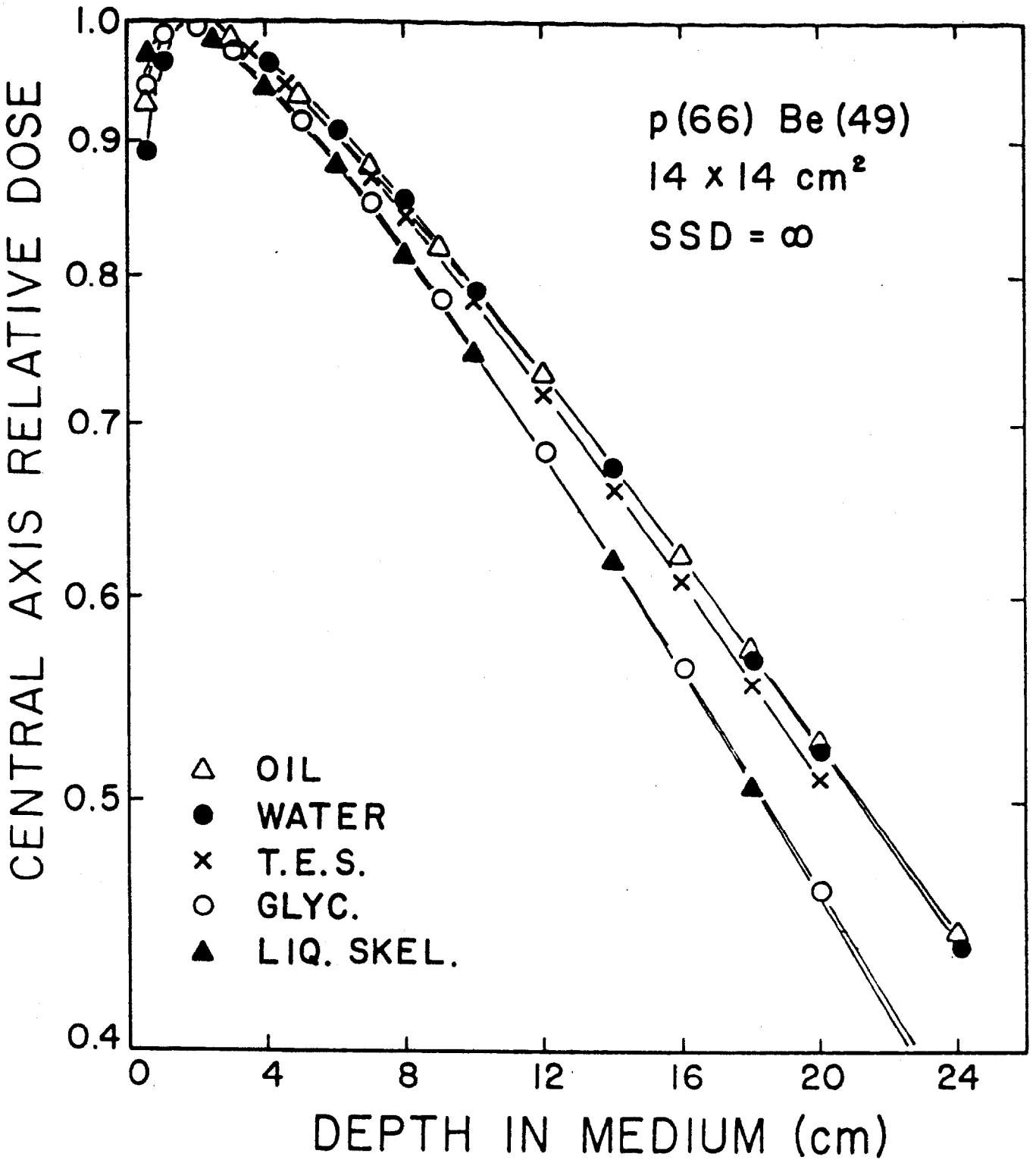
CENTRAL AXIS RELATIVE DOSE
1.0
0.9
0.8
0.7
0.6
0.5
0.4
0
4
8
12
16
20
24
DEPTH IN MEDIUM (cm)
p(66) Be(49)
14 x 14 cm²
SSD = ∞
△ OIL
● WATER
× T.E.S.
○ GLYC.
▲ LIQ. SKEL.

Fig. 1

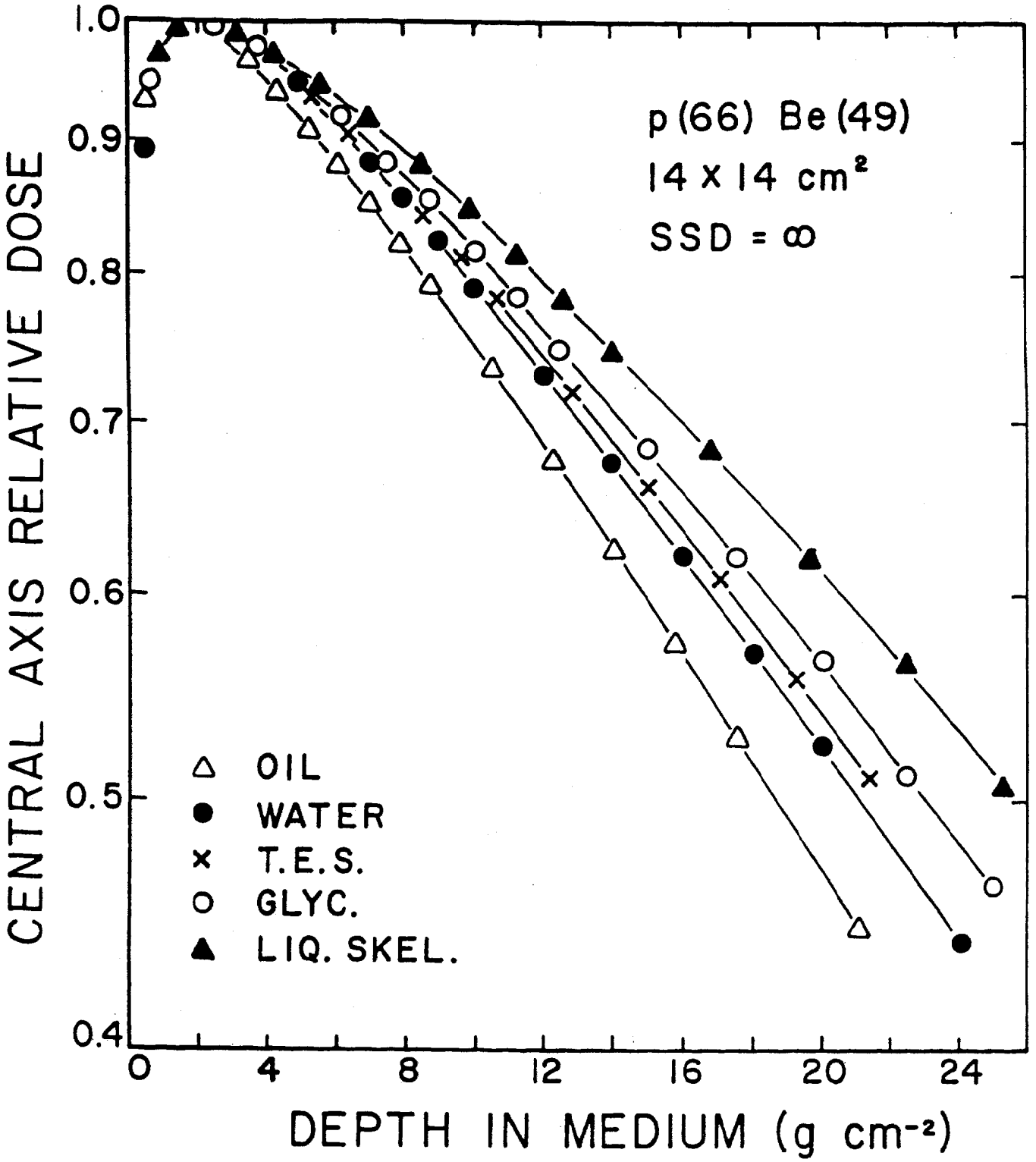
p (66) Be (49)
14 X 14 cm²
SSD = ∞
OIL
WATER
T.E.S.
GLYC.
LIQ. SKEL.
CENTRAL AXIS RELATIVE DOSE
1.0
0.9
0.8
0.7
0.6
0.5
0.4
0
4
8
12
16
20
24
DEPTH IN MEDIUM (g cm⁻²)

Fig. 2

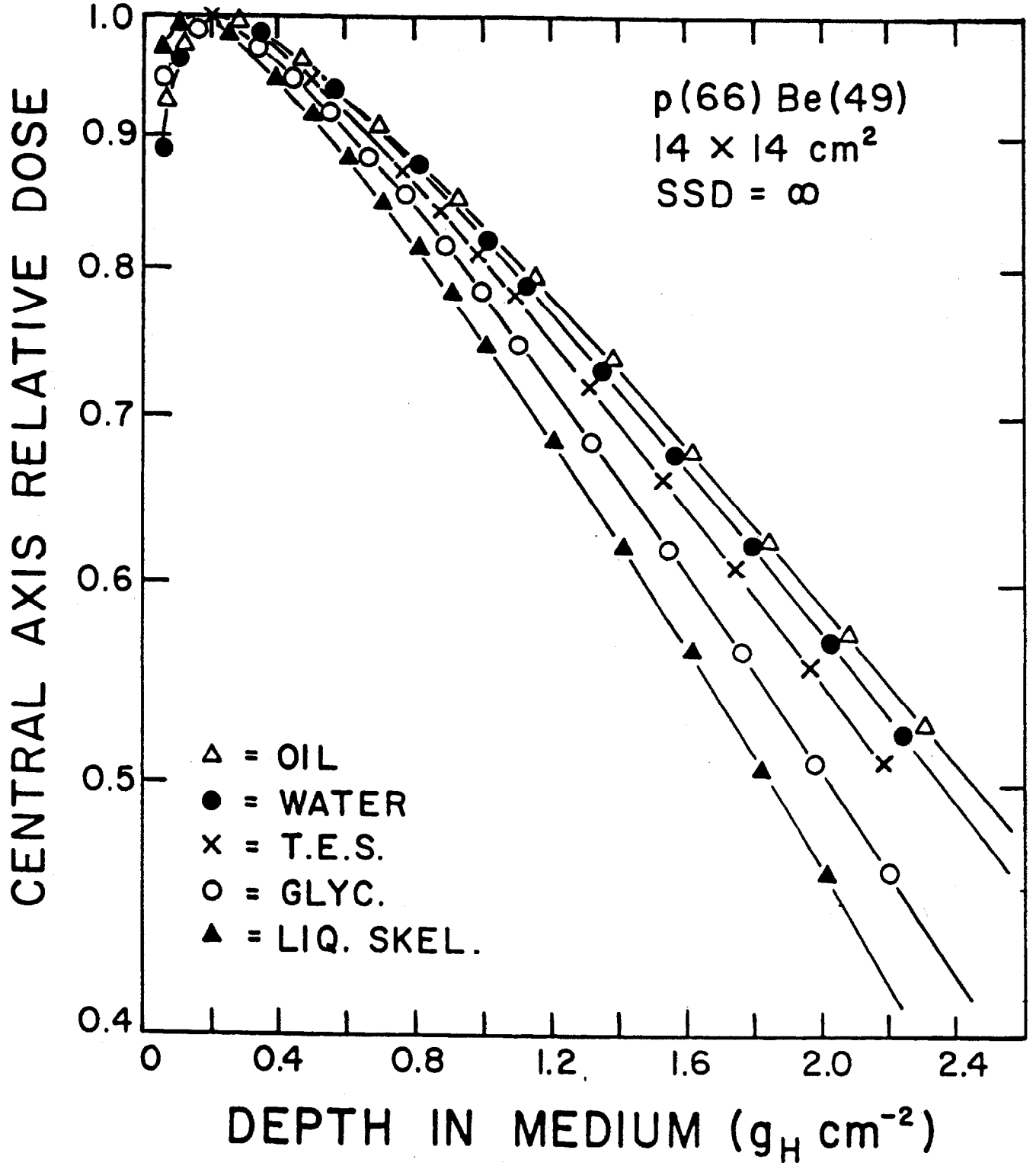
CENTRAL AXIS RELATIVE DOSE
1.0
0.9
0.8
0.7
0.6
0.5
0.4
p(66) Be(49)
14 × 14 cm²
SSD = ∞
△ = OIL
● = WATER
× = T.E.S.
○ = GLYC.
▲ = LIQ. SKEL.
0
0.4
0.8
1.2
1.6
2.0
2.4
DEPTH IN MEDIUM (g_H cm^{-2})

Fig. 3

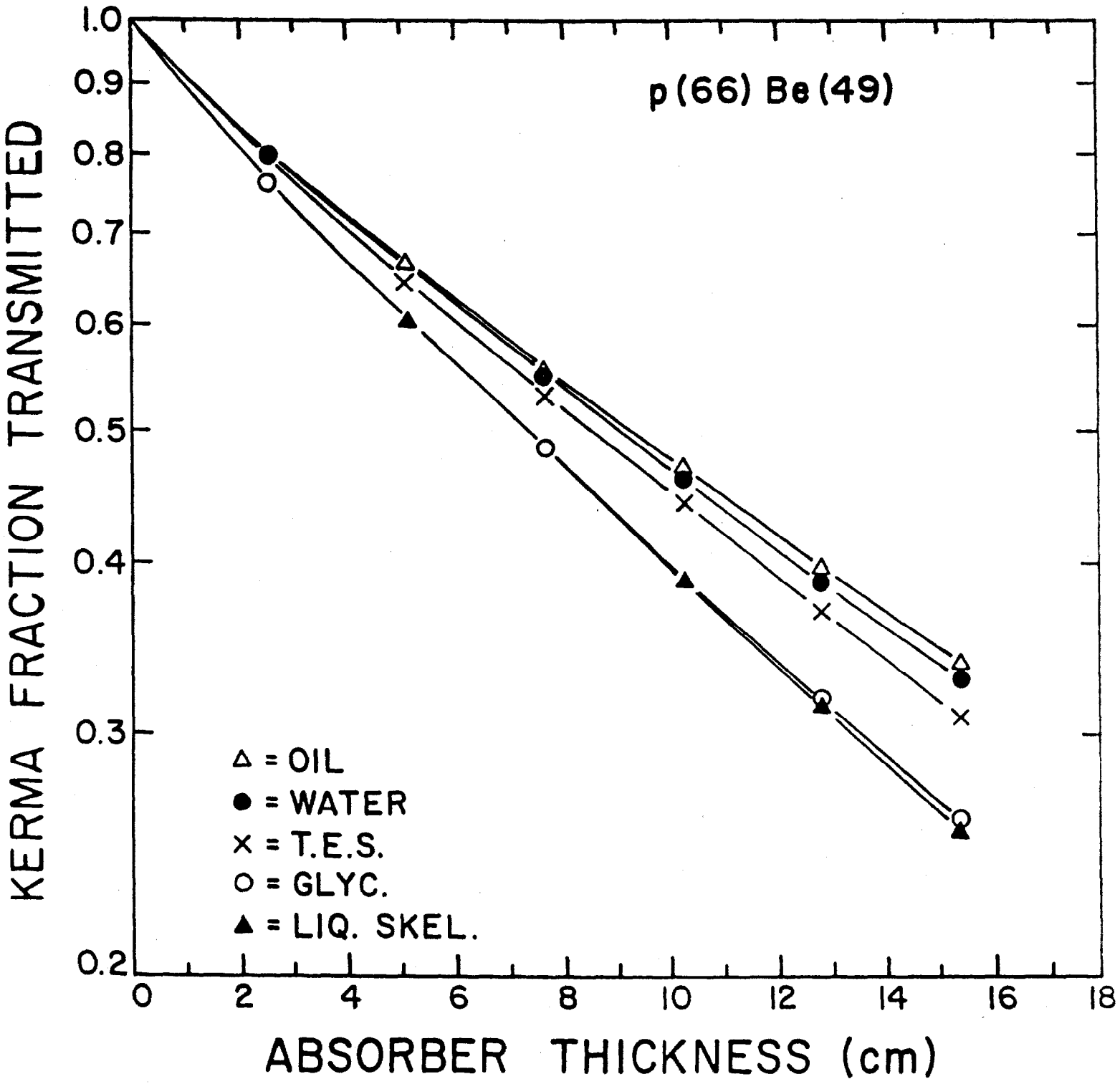
p(66) Be(49)
KERMA FRACTION TRANSMITTED
ABSORBER THICKNESS (cm)
1.0
0.9
0.8
0.7
0.6
0.5
0.4
0.3
0.2
0
2
4
6
8
10
12
14
16
18
△ = OIL
● = WATER
× = T.E.S.
○ = GLYC.
▲ = LIQ. SKEL.

Fig. 4

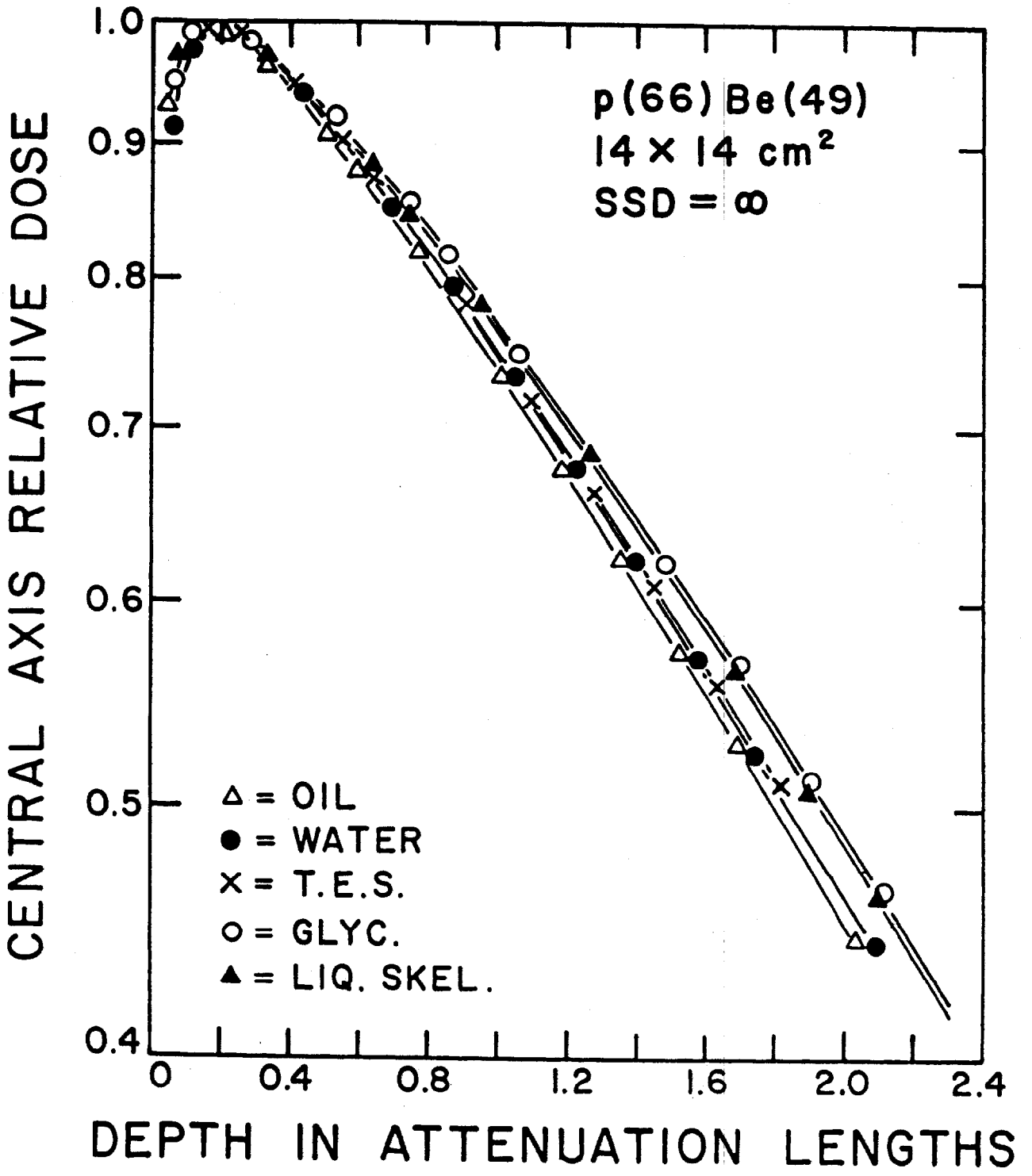
p(66) Be(49)
14 × 14 cm²
SSD = ∞
Δ = OIL
● = WATER
× = T.E.S.
○ = GLYC.
▲ = LIQ. SKEL.
CENTRAL AXIS RELATIVE DOSE
1.0
0.9
0.8
0.7
0.6
0.5
0.4
0
0.4
0.8
1.2
1.6
2.0
2.4
DEPTH IN ATTENUATION LENGTHS

Fig. 5

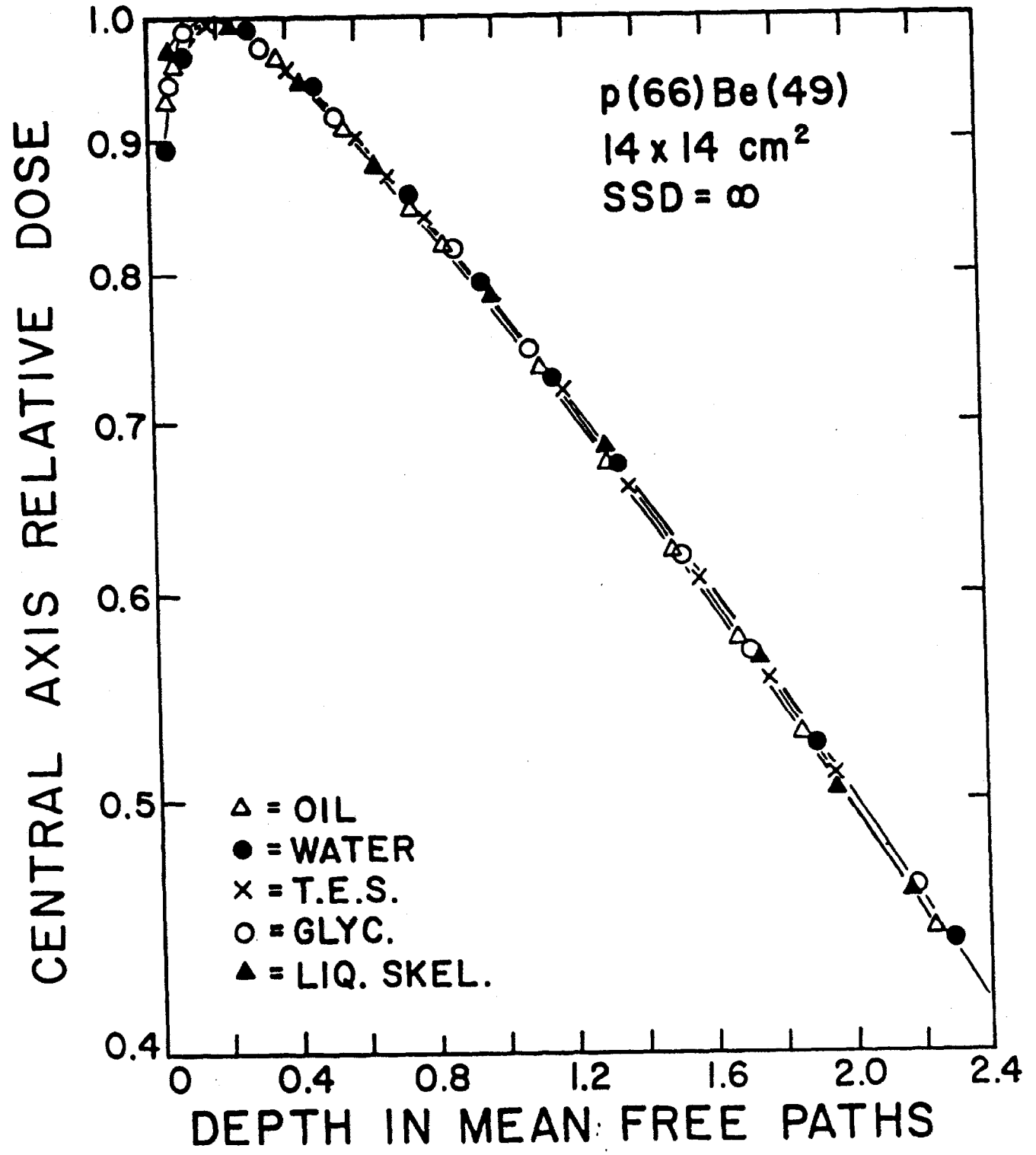
p(66)Be(49)
14 x 14 cm²
SSD = ∞
△ = OIL
● = WATER
× = T.E.S.
○ = GLYC.
▲ = LIQ. SKEL.
CENTRAL AXIS RELATIVE DOSE
1.0
0.9
0.8
0.7
0.6
0.5
0.4
0
0.4
0.8
1.2
1.6
2.0
2.4
DEPTH IN MEAN FREE PATHS

Fig. 6

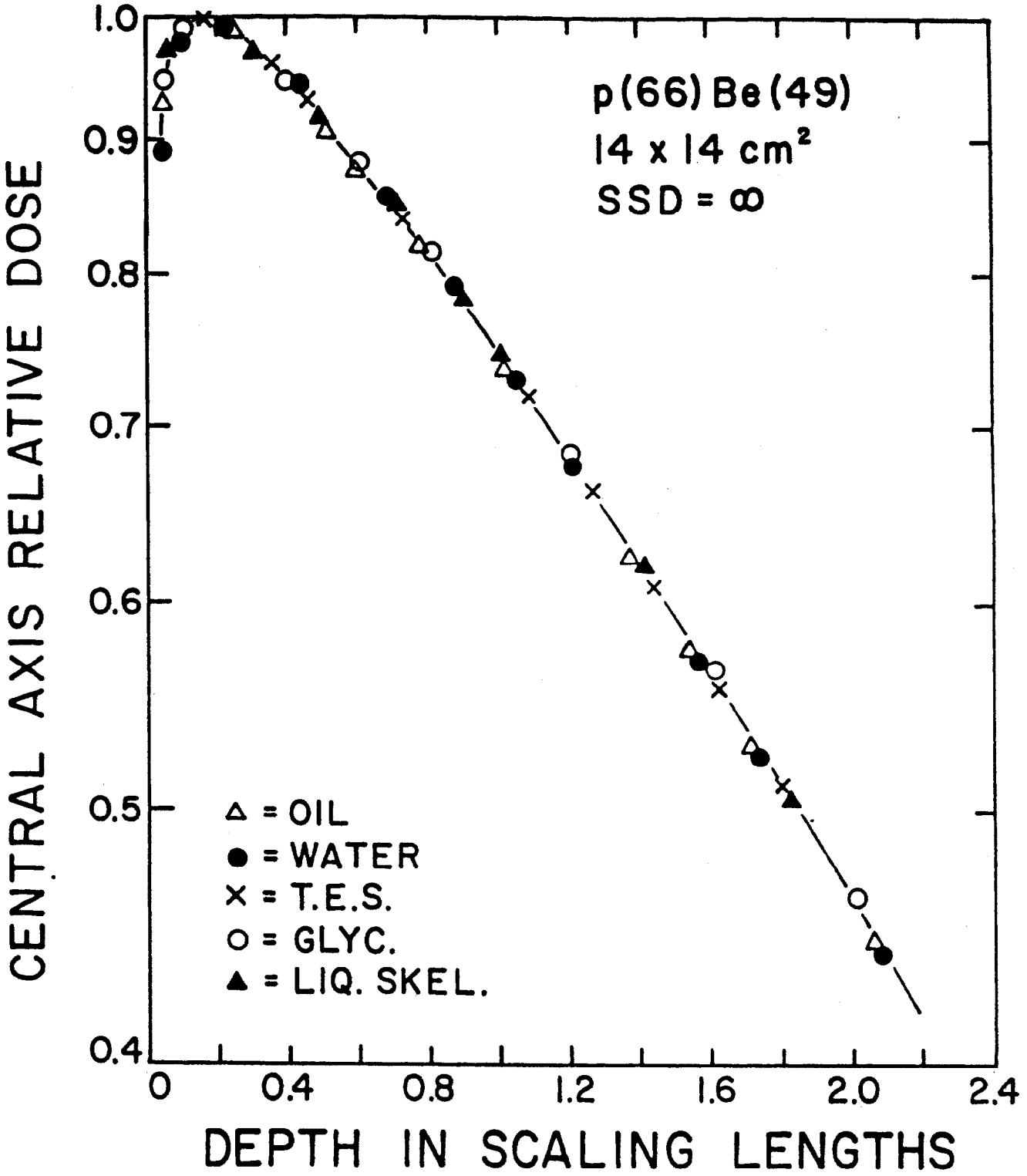
p(66) Be(49)
14 x 14 cm²
SSD = ∞
△ = OIL
● = WATER
× = T.E.S.
○ = GLYC.
▲ = LIQ. SKEL.
CENTRAL AXIS RELATIVE DOSE
1.0
0.9
0.8
0.7
0.6
0.5
0.4
0
0.4
0.8
1.2
1.6
2.0
2.4
DEPTH IN SCALING LENGTHS

Fig. 7

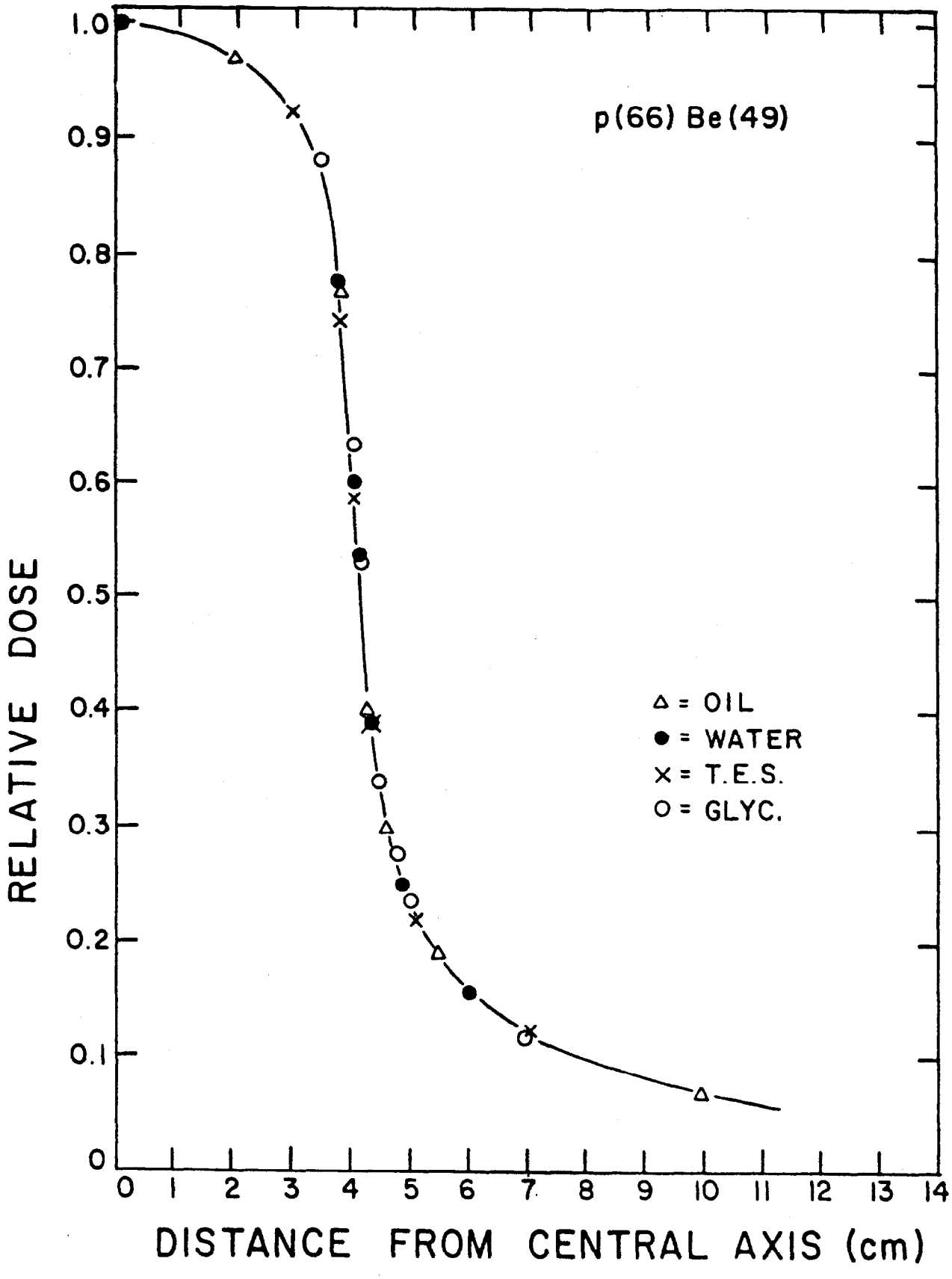
p(66) Be(49)
RELATIVE DOSE
DISTANCE FROM CENTRAL AXIS (cm)
Δ = OIL
● = WATER
× = T.E.S.
○ = GLYC.
1.0
0.9
0.8
0.7
0.6
0.5
0.4
0.3
0.2
0.1
0
0 1 2 3 4 5 6 7 8 9 10 11 12 13 14

Fig. 8

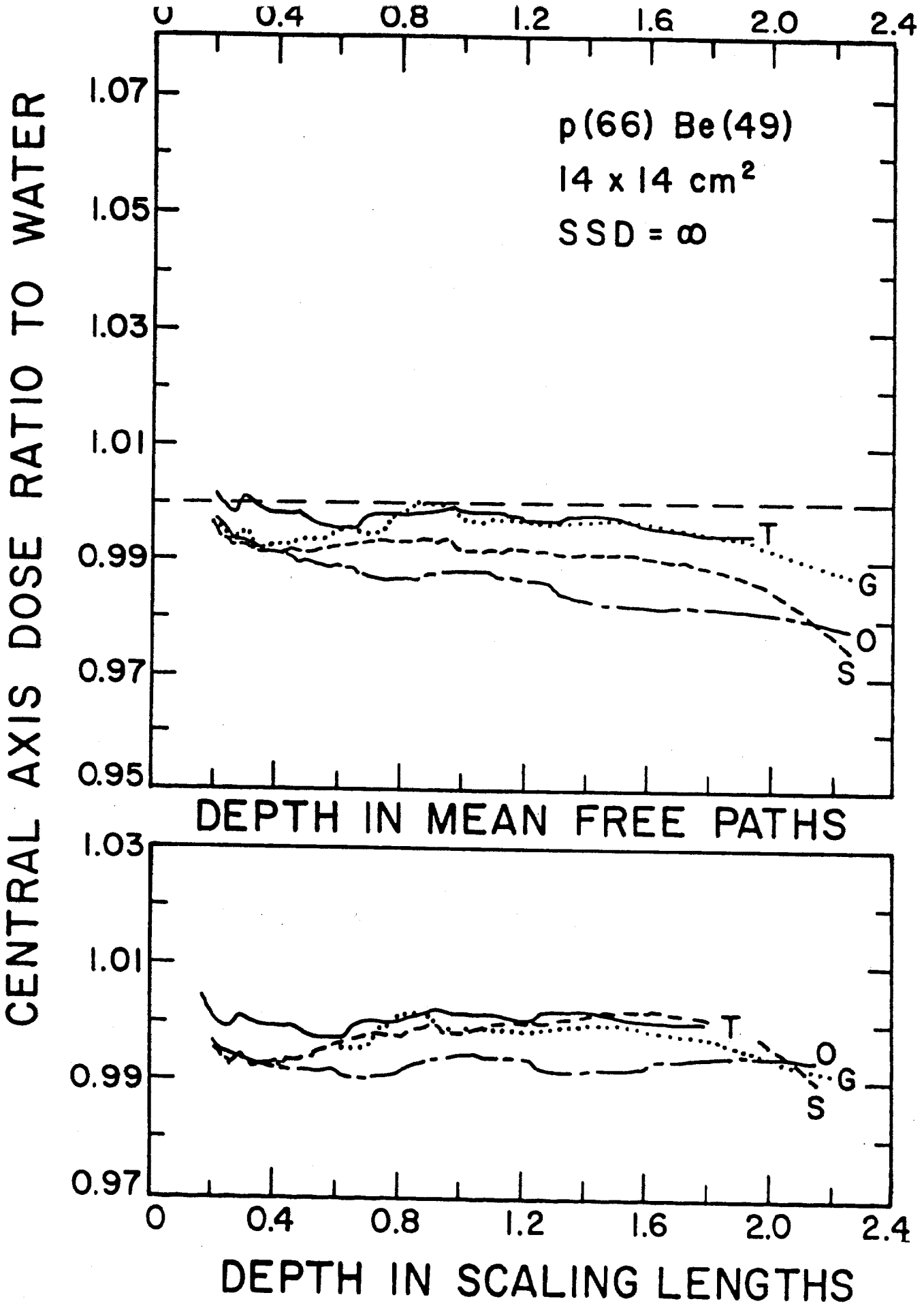
CENTRAL AXIS DOSE RATIO TO WATER
p(66) Be(49)
14 x 14 cm²
SSD = ∞
T
G
O
S
DEPTH IN MEAN FREE PATHS
DEPTH IN SCALING LENGTHS

Fig. 9

APPENDIX A

For a medium composed of several elements j, each of mass ρ_j per cm^3, the macroscopic cross-section μ for a given neutron energy spectrum N(E), is given by:

$$\mu = \sum_j n_j \bar{\sigma}_j \tag{A1}$$

and the neutron mean free path by

$$\lambda = (\mu)^{-1} \tag{A2}$$

where n_j is the number of atoms of element j per cm^3:

$$n_j = \frac{\rho_j N_a}{A_j} , \tag{A3}$$

N_a is Avogadro's number, and A_j is the atomic mass of element j.

In Eq. A1, $\bar{\sigma}_j$ is the total nuclear cross-section for the jth element averaged over the neutron energy spectrum. The usual definition of $\bar{\sigma}_j$ is:

$$\bar{\sigma}_{jl} = c_l \int_0^\infty \sigma_j(E)\ N(E)\ dE \tag{A4}$$

where $\sigma_j(E)$ is the energy dependent total cross-section of element j, and c_1 is a normalizing factor:

$$c_1^{-1} = \int_0^\infty N(E)\, dE \qquad (A5)$$

The above expression describes the average total cross-section for the attenuation of neutron fluence. However, as we are looking for a scaling length for dose attenuation in a medium and making measurements with dose-sensitive detectors (such as ionization chambers), a more appropriate definition of $\bar{\sigma}_j$ should be:

$$\bar{\sigma}_{j2} = c_2 \int_0^\infty \sigma_j(E)\, k_j(E)\, N(E)\, dE\ , \qquad (A6)$$

where $k_j(E)$ is the kerma function for element j and c_2 is now given by:

$$c_2^{-1} = \int_0^\infty k_j(E)\, N(E)\, dE \qquad (A7)$$

The above expression weighs each interaction cross-section by the energy transferred to the medium. The neutron mean free paths discussed in the text are always derived from these kerma-weighted average total cross-sections.

In addition, different average total cross-sections may be calculated to predict initial narrow beam kerma attenuation lengths.[7] These $\bar{\sigma}_j$ are weighted by the kerma response of the detector k_d used in the kerma attenuation measurements:

$$\bar{\sigma}_{j3} = c_3 \int_0^\infty \sigma_j(E)\ k_d(E)\ N(E)\ dE, \tag{A8}$$

where $k_d(E)$ is summed over the elements of the detector, i:

$$k_d(E) = \sum_i k_i(E)\ \rho_i\ \left(\sum_i \rho_i\right)^{-1} \tag{A9}$$

and c_3 is now given by:

$$c_3^{-1} = \int_0^\infty k_d(E) N(E) dE. \tag{A10}$$

The attenuation lengths, either measured or calculated using the above expressions, are evidently characteristic of the detector used as well as of the medium and the neutron energy spectrum. However, ratios of attenuation lengths, which would be used to derive scaling factors, were found to be practically independent of detector response.

APPENDIX B

The curves joining the data points in Figs. 1-3,5-7, were obtained by a quadratic polynomial interpolation to four points at a time with two points on either side of each interpolation region.[24] This method was chosen instead of the analytical function fit described in a previous report[11] in order not to prejudge the shape of the CADD curves and possibly bias subsequent analyses.

In particular, if $D_j(z_j)$ and $D_k(z_k)$ are the two interpolated CADD functions at a given SSD for media j and k, respectively, where z's are in units of length, then one can determine the values of the two transformed $CADD_\infty$'s $F_j(\beta)$ and $F_k(\beta)$ at a given "scaled depth" β, expressed in units of arbitrary scaling lengths ℓ_j and ℓ_k:

$$F_j(\beta) = D_j(z_j = \beta\ell_j) \times \frac{(SSD+z_j)^2}{(SSD+z_{jm})^2}$$

and

$$F_k(\beta) = D_k(z_k = \beta\ell_k) \times \frac{(SSD+z_k)^2}{(SSD+z_{km})^2} \qquad \text{(B1)}$$

and thus obtain a ratio function

$$R_{jk}(\beta) = F_j(\beta)/F_k(\beta). \qquad \text{(B2)}$$

This ratio function may be used to accurately determine the optimal scaling lengths which make the transformed $CADD_\infty$ functions $F(\beta)$ independent of medium and, consequently, make $R_{jk}(\beta)$ a constant for all j and k. Note that the absolute values of the scaling lengths ℓ_j and ℓ_k are not important: it is the proper ratio of ℓ's for different media that makes the function $R_{jk}(\beta)$ depth-independent. Therefore, only an optimal scaling factor

$$SF_{wj} = \frac{\ell(\text{water})}{\ell_j} \qquad \text{(B3)}$$

may be obtained empirically. Thus, ℓ(water) was arbitrarily set equal to λ(water), the calculated kerma-weighted mean free path, and the scaling lengths ℓ_j of the other media which gave the best agreement with the water data were then determined. That is, in each medium and for each measured field size and SSD, the value of SF_{wj} in Eq. B3 was varied until the resulting ratios $R_{jw}(\beta)$ became independent of β. This was determined by minimizing the absolute value of the slope of the linear regression of R_{jw} with scaled depth β. The curves of $CADD_\infty$ ratios $R_{jw}(\beta)$ obtained using

these optimal scaling lengths are shown in the bottom half of Fig. 9. These ratio functions amplify the noise inherent in the measurements, as well as the effects of discontinuities in the interpolation procedures, but it may be seen that the ratios are indeed independent of scaled depth β within those uncertainties.

Once a scaling factor S_{jk} from one medium to another is determined from the appropriate scaling lengths, i.e. $S_{jk} = \ell_j/\ell_k$, then a CADD function measured in medium j can be used to predict the CADD in medium k, using the fact that the transformed $CADD_\infty$ functions $F_j(\beta)$ and $F_k(\beta)$ in Eq. B1 are equal. Namely, the relative dose $D_k(z_k)$ at depth z_k in medium k is derived from $D_j(z_j)$ measured at depth z_j in medium j, by:

$$D_k(z_k) = D_j(z_j) \frac{(SSD+z_j)^2}{(SSD+z_k)^2} \qquad \text{(B4)}$$

where

$$z_j = z_k S_{jk} = z_k(\ell_j/\ell_k)$$

assuming the depths for maximum dose z_m are about equal, all z's being expressed in centimeters.

REFERENCES

1. American Association of Physicists in Medicine Report No. 7, Protocol for Neutron Beam Dosimetry, New York: American Institute of Physics, 1980.

2. Broerse, J. J., Mijnheer, B. J., Williams, J. R., European Protocol for Neutron Dosimetry for External Beam Therapy, Brit. J. Radiol. 54, 882 (1981).

3. Goodman, L. J., A Modified Tissue-Equivalent Liquid, Health Phys. 16, 763 (1969).

4. Frigerio, N. A., Coley, R. F., Sampson, M. J., Depth Dose Determination I. Tissue Equivalent Liquids for Standard Man and Muscle, Phys. Med. Biol. 17, 792 (1972).

5. ICRP Report No. 23, Report of the Task Group on Reference Man, International Commission for Radiological Protection, New York: Pergamon Press, 1975.

6. ICRU Report No. 26, Washington DC, International Comm. Radiat. Units and Meas., Jan. 1977.

7. Awschalom, M., Hrejsa, A., Rosenberg, I., Ten Haken, R. K., Kerma Transmission Through Various Materials for a p(66)Be(49) Neutron Beam, Health Phys. 41, 184 (1981).

8. Cohen, L., Awschalom, M., The Cancer Therapy Facility at the Fermi National Accelerator Laboratory, Batavia, Illinois, A Preliminary Report, Applied Radiology 5, 51 (1976).

9. Awschalom, M., Grumboski, L., Hrejsa, A. F., Lee, G., Rosenberg, I., The Fermilab Cancer Therapy Facility: Status Report After 2.5 Years of Operation, IEEE Trans. Nucl. Sci. NS-26 #3, 3068 (1979).

10. Awschalom, M., Rosenberg, I., Neutron Beam Calibration and Treatment Planning, Fermilab Internal Report TM-834, Dec. 1978.

11. Rosenberg, I., Awschalom, M., Characterization of a p(66)Be(49) Neutron Therapy Beam: I. Central Axis Depth Dose and Off-Axis Ratios, Med. Phys. 8, 99 (1981).

12. Awschalom, M., Goodwin, R., Grumboski, L., Rosenberg, I., Shea, M., High Precision in Dose Delivery: Routine Use of a Microcomputer, in Biomedical Dosimetry: Physical Aspects, Instrumentation, Calibration, Vienna: IAEA, 1982, pp. 271-280.

13. Constantinou, C., Phantom Materials for Radiation Dosimetry. I. Liquids and Gels. Brit. J. Radiol. 55, 217 (1982).

14. Sears, Roebuck, and Co., Chicago, IL, 10W-30 motor oil.

15. Smathers, J. B., Otte, V. A., Smith, A. R., Almond, P. R., Attix, F. H., Spokas, J. J., Quam, W. M., Goodman, L. J., Composition of A-150 Tissue Equivalent Plastic, Med. Phys. 4, 74 (1977).

16. Rosenberg, I., Awschalom, M., Ten Haken, R. K., The Effect of Missing Backscatter on the Dose Distribution of a p(66)Be(49) Neutron Therapy Beam, Med. Phys. 9, 559 (1982).

17. T-2 ionization chamber made by Exradin, Inc., Warrenville, Illinois.

18. EG&G Model IC-18, now made by Far West Technology, Goleta, CA 93017.

19. Ten Haken, R. K., Awschalom, M., Rosenberg, I., Kerma Transmission Through Steel for a p(66)Be(49) Neutron Beam: An Update, to appear in Health Phys. (1983).

20. Rosenberg, I., Awschalom, M., Ten Haken, R. K., The Effects of Hydrogenous and Non-Hydrogenous Filters on the Quality of a p(66)Be(49) Neutron Beam, Med. Phys. 9, 199 (1982).

21. EG&G Model IC-17, now made by Far West Technology, Goleta, CA 93017.

22. Awschalom, M., Rosenberg, I., Mravca, A., Kermas for Various Substances Averaged Over the Energy Spectra of Fast Neutron Therapy Beams: A Study in Uncertainties, Fermilab TM-1086. To appear in Med. Phys. 10 (1983).

23. Hughes, D. J., Schwartz, R. B., Neutron Cross-Sections, 2nd edition, Brookhaven National Laboratory publication BNL-325. USAEC (1958), and Hughes, D. J., Magurno, B. A. and Brussel, M. K., Suppl. Number 1 to above (1969).

24. Awschalom, M., Rosenberg, I., Ten Haken, R. K., A New Look at Displacement Factor and Point of Measurement Corrections in Ionization Chamber Dosimetry, to appear in Med. Phys. 10 (3) (1983).